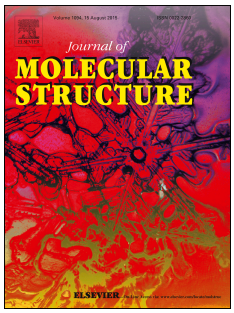

Synthesis, structural characterization, DFT and molecular simulation study of new zinc-Schiff base complex and its application as a precursor for preparation of ZnO nanoparticle

Masumeh Galini, Mehdi Salehi, Maciej Kubicki, Mehdi Bayat, Rahime Eshaghi Malekshah

PII: S0022-2860(20)30039-9

DOI: https://doi.org/10.1016/j.molstruc.2020.127715

Reference: MOLSTR 127715

To appear in: *Journal of Molecular Structure*

Received Date: 14 July 2019

Revised Date: 8 January 2020

Accepted Date: 8 January 2020

Please cite this article as: M. Galini, M. Salehi, M. Kubicki, M. Bayat, R.E. Malekshah, Synthesis, structural characterization, DFT and molecular simulation study of new zinc-Schiff base complex and its application as a precursor for preparation of ZnO nanoparticle, *Journal of Molecular Structure* (2020), doi: https://doi.org/10.1016/j.molstruc.2020.127715.

Graphical abstract

The complex [ZnL(2-ampy)Br] was synthesized and structurally characterized. The crystal of complex was determined by single X-ray diffraction study. Docking calculations of these complex were performed to explore the exact binding sites. The nature of the Zn→L bonds in the compound was analyzed with NBO, EDA analyses and molecular docking. The ZnO nanoparticles were prepared via combustion method of the complex at 700℃ for 8 h. Finally, crystallinity, purity, and morphology of the ZnO nanoparticles were characterized by FT-IR, XRD, FESEM, and TEM.

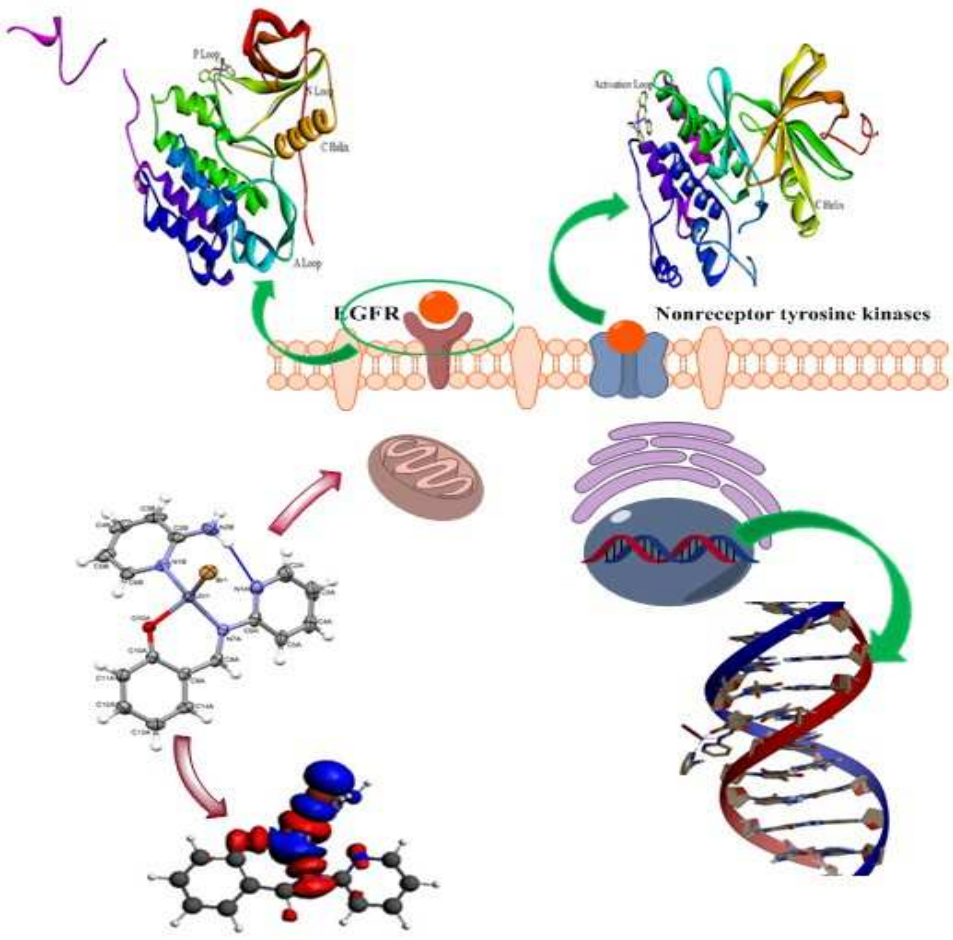

Synthesis, structural characterization, DFT and molecular simulation study of new zinc-Schiff base complex and its application as a precursor for preparation of ZnO nanoparticle

Masumeh Galini[a], Mehdi Salehi [a,]*, Maciej Kubicki[b], Mehdi Bayat[c], Rahime Eshaghi Malekshah[a]

[a]*Department of chemistry, Semnan University, Semnan 35351-19111, Iran*

[b]*Faculty of Chemistry, Adam Mickiewicz University, Umultowska 89b, 61-614 Poznan, Poland*

[c]*Department of Inorganic Chemistry, Faculty of Chemistry, Bu-Ali Sina University, Hamedan 65167, Iran*

Abstract:

In this study, the metal complex [ZnL(2-aminopyridine)Br] (**I**) was synthesized from a metal salt with Schiff base ligand (HL). The synthesized complex (**I**) was elucidated by using FT-IR, UV-Vis spectroscopy, ^{1}H-NMR, and. Moreover, the crystal structure of the complex was determined by X-ray analysis and revealed the complex has a distorted tetrahedral coordination structure. The stimulation revealed the binding pattern of this compound with BNA that the free energy (ΔG) of interaction is −7.73 kcal/mol. Also, free energy (ΔG) of complex (**I**) with EGFR-TKD, ABL/dasatinib complex and the ABL/imatinib complex was by -6.47, - 5.20 and - 6.60 kcal/mol. Then, the nature of the Zn→L bonds in the complex (**I**) was analyzed with NBO and EDA analyses. In the next step, ZnO nanoparticles were prepared via combustion synthesis method of the complex (**I**) at 700℃ for 8 h. Finally, crystallinity, purity, and morphology of the ZnO nanoparticles were characterized by FT-IR, XRD, FESEM, and TEM.

Keywords: Crystal structure**,** ZnO nanoparticles**,** Hydrolytic cleavage**,** Molecular docking, Non-receptor tyrosine kinases, Receptor tyrosine kinases.

1. Introduction

The discovery of new transition metal complexes with Salicylaldehyde Schiff base played a significant role in the growth and development of coordination chemistry for their applications, properties and interesting structures [1-3]. The discovery of new transition metal complexes with Salicylaldehyde Schiff base explicate the mechanism of transamination reactions in biological system [4-6]. Among these complexes, Schiff base zinc complexes, especially chiral Zn(II) complexes have been attracted much attention because of their physiological and pharmacological activities[7]. Also, the synthesis of several salicylaldehydes and 2-Aminopyridine derivatives−Schiff base from the simple condensation and their complex was reported [8-11]. The theoretical studies of the ground state intramolecular proton transfer (IPT) and solvation effect have also been reported from 2-aminopyridine with 2-hydroxy-1-naphthaldehyde and 2-hydroxy salicylaldehyde [12]. Zhu et al. studied synthesis and crystal structure of polynuclear tridentate with cobalt(II) sulfate and cobalt(II) perchlorate [13]. In the other article, the biological properties of binuclear Ru(II) complexes with Schiff bases derived from 5-chlorosalicyladehyde and 2-aminopyridine and its 5-substituted salicylideneimine homologues were reported [14]. Giri et al. synthesized a tetranuclear Cu(II) complex $[Cu_4L_4(H_2O)_4](ClO_4)_4$ using the terdentate Schiff base 2-(pyridine-2-yliminomethyl)-phenol (HL) [15]. In addition to, antimicrobial activity of copper(II) complex of Schiff base derived from 2-(salicylidene) aminopyridine was tested in comparison with the activity of the corresponding Schiff base [16]. Tyagi et. al. reported Ni(II) and Zn(II) metal complexes of Schiff base and tested cytotoxic activity of against human breast cancer cell line (MCF-7) and human

hepatocellular liver carcinoma cell line (HepG2). Also, The DFT studies of Schiff bases and metal complexes has been assigned for Co(II), Ni(II) Cu(II) and Zn(II) complexes using the 6-31+g(d,p) basis set. The theoretical results certainly supported experimental data confirms the suggested structure [17]. In another study, Zn(II) complex was analysed using molecular dynamics simulation and molecular docking studies. Molecular docking studies shown Zn(II) complex located to the major groove [18]. So far, the Schiff base zinc complexes containing the bromide ligands and salicylaldehyde have rarely been reported. Furthermore, among transition metal oxides, zinc oxide have attracted increasing attention for its unique physical and chemical properties such as gaseous sensors [19], photocatalysts [20], and additives in many industrial products [21]. There are several methods to prepare nanostructured ZnO such as solvothermal and hydrothermal [22-24], sol-gel [25], polymerization [26], and mechanochemical methods [27]. This work, FT-IR, ultraviolet-visible spectra (UV-Vis), and X-ray were used to describe the structure of new complex (**I**). In addition, the nature of the Zn→L bonds in the complex was analyzed with NBO (The Natural Bond Orbital) and EDA (energy and decomposition analysis) techniques. Furthermore, ZnO nanoparticles were successfully prepared via combustion synthesis method of the complex (**I**) (Scheme 1). The morphology and structure of the as-prepared ZnO were investigated by FESEM, TEM, XRD, and FT-IR spectra. Eventually, the docking study of selected compound with (PDB ID: 1BNA), the epidermal growth factor receptor (EGFR-TKD) (PDB ID: 1M17), the ABL/dasatinib complex (PDB ID: 2GQG) and the ABL/imatinib complex (PDB ID: 2HYY) were accomplished in order to predict the chosen binding site.

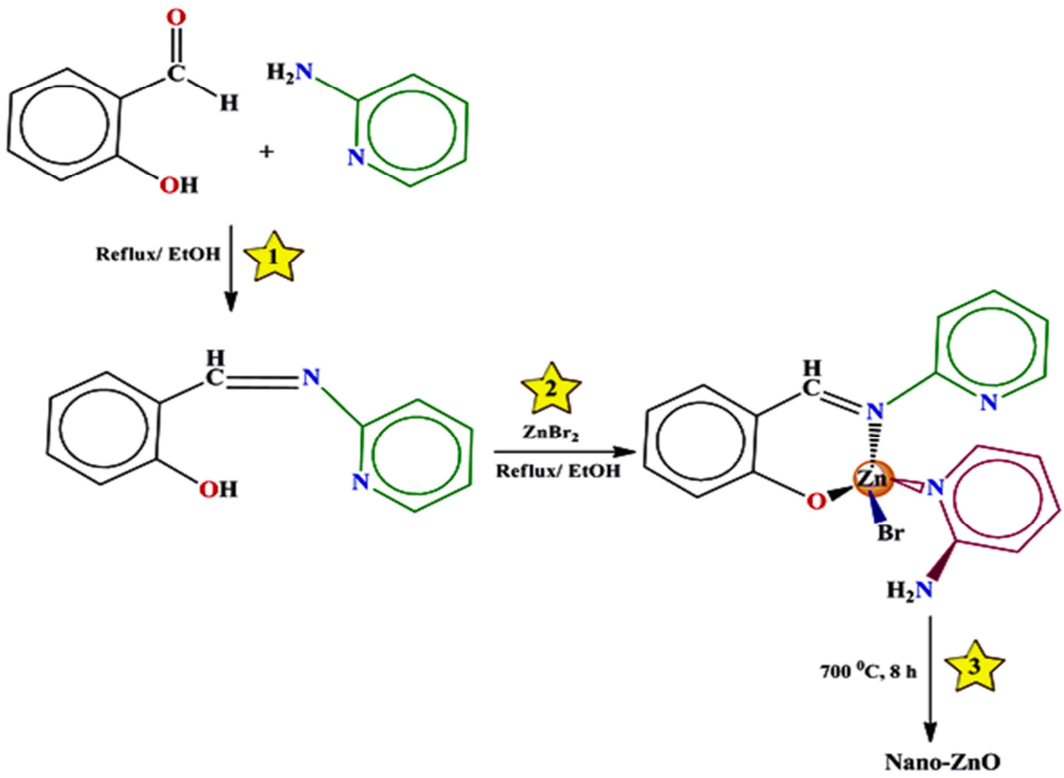

Scheme 1. Synthetic procedure for the preparation of Schiff base ligand and complex (2:1) and protocol of ZnO nanoparticles.

2. Experimental

2.1. Materials and methods

All the materials in the experiment were purchased from Aldrich and Merck and used without further purification. FT-IR spectra in KBr plates were performed on FT-IR SHIMADZU spectrophotometer in 4000-400 cm^{-1}. UV-Vis spectra were recorded on a UV-1650 PC SHIMADZU spectrophotometer in methanol (MeOH) solution. ^{1}H-NMR measurements were recorded with the NMR BRUKER 300MHz spectrometer, using deuterated methanol (CD_3OD) as the solvent. Also, the crystallographic information and phase purity of the nanostructure were acquired with the X-ray powder diffraction (XRD) using Bruker D8000 Germany in a scanning range of 2θ = 10–90^o and CuK_α radiation. The morphological and structural characteristics, as

well as particle size distribution of the nanostructures of ZnO, were investigated using the field emission scanning electron microscope (FESEM, Hitachi model S-4160) and a transmission electron microscopy (TEM, Philips-CM300).

2.2. Synthesis of the Schiff-base ligand HL

The Schiff-base ligand **HL** was performed according to the literature procedure [28]. The ligand was prepared by condensing salicylaldehyde with 2-aminopyridine in 1:1 molar ratio in 20 mL EtOH. The reaction solution was refluxed at room temperature for 3 h. The orange crystalline powder separated by a Buchner funnel, washed with absolute ethanol, and dried under vacuum. Mol. Wt.: 198.22 g/moL. mp. 70 ℃. FT-IR: ν_{max} cm^{-1} (KBr): 1608 (s, C=N), 1556, 1573 (s, C=C_{arom}), 1278 (s, C-O). UV–Vis: λ_{max} (nm) (ε, $M^{-1}cm^{-1}$) (MeOH): 347(25300), 295(29900), 268(29800), 221(38600). ^{1}HNMR ($CDCl_3$, 400 MHz): 6.91-8.57(m, 8H), 9.52(s, 1H), 13.05(s, 1H).

2.3. Synthesis of the Complex [ZnL(2-aminopyridine)Br] (I)

An ethanol solution (5 mL) of $ZnBr_2$ (0.225 g, 1 mmol) was added dropwise into the ethanol solution (15 mL) of Schiff base ligand HL (0.396 g, 2 mmol). The resulting yellow mixture was refluxed for 3 h, then allowed to cool down at room temperature. The single yellow crystals suitable for X-ray data collection were obtained by slow evaporation after 2 days. The crystals were separated, washed with a small amount of cold pure ethanol, and dried under vacuum. Mol. Wt.: 436.62 g/moL. mp. 220 ℃, FT-IR: ν_{max} cm^{-1} (KBr): 1614 (s, C=N), 1496, 1529 (s, C=C_{arom}), 1263 (s, C-O). UV–Vis: λ_{max} (nm) (ε, M^{-1} cm^{-1}) (MeOH): 405(12300), 300(29200), 232(39400).^{1}H-NMR (CD_3OD, 300 MHz): 6.6(m, 12H), 4.8(s, DOH), 9.2(s, 1H).

2.4. Preparation of ZnO nanostructure of the complex (I)

An appropriate amount of complex (**I**) powder (1g) as the precursor for ZnO was weighed and transferred into a crucible. The crucible containing complex was heated at 700℃ for 8 h. Then, the white powder obtained from the calcination complex was collected for characterization.

2.5. X-ray crystallography

Diffraction data were collected by the ω-scan technique at room temperature on Rigaku Xcalibur four-circle diffractometer with Eos CCD detector and graphite-monochromated MoK_{α} radiation (λ=0.71069 Å). The data were corrected for Lorentz-polarization as well as for absorption effects [29]. Precise unit-cell parameters were determined by a least-squares fit of 4109 reflections of the highest intensity chosen from the whole experiment. The structure was solved with SIR92 [30] and refined with the full-matrix least-squares procedure on F^2 by SHELXL-2013 [31]. All non-hydrogen atoms were refined anisotropically, hydrogen atoms from NH_2 group were found in difference Fourier maps and isotropically refined, all other hydrogen atoms were placed in idealized positions and refined as 'riding model' with isotropic displacement parameters set at 1.2. The crystallographic and refinement data are summarized in Table 1.

Table 1.

Crystallographic data for the structural analysis has been deposited with the Cambridge Crystallographic Data Centre, Nos. CCDC-1534258. Copies of this information may be obtained free of charge from: The Director, CCDC, 12 Union Road, Cambridge, CB2 1EZ, UK. Fax: +44(1223)336-033, e-mail:deposit@ccdc.cam.ac.uk, or www: www.ccdc.cam.ac.uk.

2.6. Computational methods

The geometries of the compound investigated here were optimized without symmetry constraints at the BP86 [32-33]/def2-SVP [34] level of theory using the Gaussian03 software [35]. It has been shown that BP86 is a suitable level for calculation of bonding situation M←L among these

complexes [36-40]. Vibrational frequency analyses, calculated at the same level of theory, indicate that the optimized structures are at the stationary points corresponding to local minima without any imaginary frequency. The geometry of the metal complex (**I**) was determined by the X-ray crystal structure analysis (Fig. 3) and was fully optimized at the above-mentioned level of theory. NBO analyses were also carried out with the internal model GAUSSIAN 03. The bonding analysis in terms of energy-decomposition analysis was carried out at BP86/TZ2P(ZORA)//BP86/def2-SVP with C_1 symmetry. The basis sets for all elements have triple-f quality augmented by one set of polarization functions (ADF basis set TZ2P(ZORA)) with the program package ADF 2009.01. EDA calculations were carried out to analyze the nature of bonds between the $[ZnPy(R)]^+$ and $[L]^-$ (Schiff base ligand) fragments in the complex (**I**).

2.7. Docking Studies

To investigate antitumor activity, the possible basis in target sites, best orientation of the molecule, and targeted therapeutic strategies of compounds, we used computational approaches. The metal complex was used from their crystal structure as a CIF file and converted to the PDB format using Mercury software 1.4.2. The crystal structure of the B-DNA dodecamer d(CGCGATATCGCG)2 (PDB ID: 1BNA) [41], crystal structure of the epidermal growth factor receptor (EGFR-TKD) (PDB ID: 1M17), the ABL/dasatinib complex (PDB ID: 2GQG) and the ABL/imatinib complex (PDB ID: 2HYY) were retrieved from the protein data bank (http://www.rcsb.org./pdb). Molecular docking study of complex Zn(II) with protein tyrosine kinase, drugs of anticancer (Afatinib, Erlotinib, Gefitinib) with the epidermal growth factor receptor was implemented using AutoDock 4.2 calculations (The Scripps Research Institute, La Jolla, CA, USA). All water molecules of receptor were removed. The Zn(II) complex was

enclosed in a box with number of grid points in x×y×z directions (74×64×117 Å) with a grid-point spacing of 0.991 Å for 1BNA, A grid box of the size 126 × 126 × 126 Å with a grid-point spacing of 0.502 Å for the epidermal growth factor receptor (EGFR) and a grid box of the size 126 × 126× 126 Å with a grid-point spacing of 0.991 Å for GQG and a grid box of the size 126 × 126× 126 Å with a grid-point spacing of 0.825 Å for 2HYY were selected for docking purpose. The best optimized model having lowest energy was picked up from the one minimum energy (root mean square deviation, RMSD = 0.0) from the 100 runs to compare the structural similarity [42]. Then, the interactions of protein tyrosine kinase and non-receptor tyrosine kinases with complex (**I**) were analyzed Discovery Studio 3.0 Accelrys and DS Visualizer.

3. Results and discussions

3.1. Synthesis

The new complex (**I**) was synthesized and characterized by FT-IR, ^{1}H-NMR, UV-Vis, and X-ray analysis. It is worth mentioning that this complex is completely soluble in common organic solvents such as methanol, ethanol, and chloroform. Some spectroscopic data for ligand and metal complex in Table S1 are in good agreement with the expected values.

3.2. Spectroscopic characterization of the complex (I)

3.2.1. FT-IR spectra

The FT-IR spectra of HL and the complex **I** provide useful information about the metal-ligand bonding, with results summarized in Table S1. The absorption peaks in the area around 3334 and 3415 cm^{-1} indicate the existence of NH_2 group in the complex [43], emphasizing that the amino N-atom is not participating in bonding [44]. Therefore, this observation is appropriate with the X-ray crystal structure of the complex that shows coordination of the 2-aminopyridine ligand only through the pyridine N-atom. The FT-IR spectra of the free ligand reveal that a band

at 3051 cm^{-1} may be assigned to υ(OH), which is absent in the spectrum of complex, indicating coordination through the deprotonated phenolic OH group [45, 46]. The absorption band in the ligand attributed to the phenolic oxygen (C-O) group that was shifted to a lower frequency in the complex. The infrared spectra of the ligand showed a band at 1608 cm^{-1} assigned to the azomethine group υ(C=N) while this band in the spectrum of the complex was shifted to the higher frequency 1614 cm^{-1}, due to participation the nitrogen of azomethine group in coordination [46-48].

3.2.2. Electronic spectra

The electronic spectra of the free Schiff base ligand and its complex in methanol solution are shown in Fig S1. The electronic spectrum of free ligand shows four bands in the regions 221, 268, 295, and 347 nm, with the three first band indexed to the $\pi \rightarrow \pi^*$ transition of the aromatic ring and the azomethine chromophore and the last band corresponding to $n \rightarrow \pi^*$. In complex (**I**), the band at 405 nm can be assigned to the charge-transfer (CT) transition by metal-to-ligand (MLCT) π-back bonding, which is absent for the HL ligand.

3.2.3. ^{1}H-NMR spectra of Schiff base ligand and complex (I)

The ^{1}H-NMR spectra of the Schiff base ligand and its complex (**I**) were recorded in CD_3OD solution (Fig.s S2 and S3). The position of the imine proton (CH=N) signal and O-H signal of Schiff base ligand observed at 9.52 and 13.05 ppm, respectively [49, 50]. While, the multiplets of aromatic protons are in the region between 6.91-8.57 ppm [51, 52]. The signal of the imine proton and the phenolic OH disappeared in the spectrum of the complex. Disappearing Phenolic-OH signal (hydroxyl protons) corresponded to deprotonation of phenolic proton and confirmed coordination through phenolic oxygen to the metal ions. Also, due to the a peak at 4.84 ppm region, corresponded to DOH proton

3.3.3. Description of the crystal structures

The perspective view of the complex (**I)** is shown in Fig. 1, some geometrical data are listed in Table 2. Zn cation is 4-coordinated, by two atoms (N and O) of ligand molecule, a nitrogen from coordinated 2-aminopyridine molecule and a bromine atom, in a distorted tetrahedral fashion (bond angles are in the range 93.48(10)º-123.16(11)º). The ligand molecule is only slightly folded and the dihedral angle between the terminal ring planes is 11.76(17) º. The intramolecular N-H···N hydrogen bond, with the ring nitrogen of the L molecule (not involved in coordination) is possible because the coordinated pyridine ring is twisted by *ca.* 60º with respect to the L molecule.

In the crystal structure (Fig. 2) the N-H···Br hydrogen bonds connect molecules into infinite chains along x-direction. Both intra- and intermolecular interactions are enforced by secondary C-H···O, weak hydrogen bonds. Table 3 lists the hydrogen bond data.

Fig.s 1-2

Tables 2-3

3.3.4. Theoretical studies

The molecular structure of the complex (**I**) which determined by the X-ray crystal structure (see Fig. 1), and fully optimized at BP86/def2-SVP level of theory. Data show that in above complex similar to that obtained by X-ray crystal structures, one nitrogen and one oxygen atoms from the Schiff base ligand, one nitrogen from pyridine group and also one bromine atom are arranged around the Zn(II) within a distorted tetrahedral geometry (Fig. 3). Selected calculated bond lengths and bond angles of complex (**I**) are given in Table 4. As it can be seen, the calculated bond length of Zn←N_2 and Zn←N_3 which obtained from σ-donation of N atom of Schiff base and pyridine ligands to metal ion are about 0.05 and 0.06 Å larger than experimental

data (See Table 4). Also the Zn–O_1 bond length in the complex which obtained from σ-donation of O atom of phenoxide group to metal ion is about 0.06 larger than experimental data. Some selected optimized and X-ray experimental values of bond lengths and bond angles around the metal ion are respectively shown in Table 2 for complex (**I**)**.** The optimized values are similar to that obtained with experimental data. In continuation, two interacting fragments, $[ZnPy(R)]^+$ and $[L]^-$ (Schiff base ligand) in the complex (**I**) are considered and nature of bonds between mentioned fragments are studied with the help of NBO analysis. The values of natural charges on Zn metal ion and N, O and Br atoms as well as total charge of $[L]^-$ ligand(Schiff base ligand) in the complex are also studied (Table S2).

The observed data confirms that the Zn(II) metal ion is carried the positive and N, O Br and Schiff base ligand are carried negative natural charges respectively. Also the values of charge transfer from L ligand (Schiff base ligand) to $[ZnPy(R)]^+$ fragment in the complex is about -0.42e. The Wiberg bond indices (WBIs) for Zn→L bonds are calculate and corresponding values are included in Table 4. The values of WBIs for Zn→N_2 and Zn→O_1 bonds in the complex are about 0.30 and 0.32 respectively. Also in the complex the value of M→N bonds obtained from Schiff base ligand is similar to that obtained from pyridine group (Table 4).

In recent years, Morokuma [53] and Ziegler et al [54] presented the "energy decomposition analysis" (EDA) method. With the help of this technique, we could explain the strength of M←L σ donation and M→L back bonding in the complexes [53-57].

To better relalized the nature of the bond between two interacting fragments, $[ZnPy(R)]^+$ and $[L]^-$ ligand(Schiff base ligand) in complex (**I**), the energy-decomposition analysis (EDA) is carried out at BP86/TZ2P(ZORA)//BP86/def2-SVP with C_1 symmetry. The results indicated that the ΔE_{int} for complex (**I**) is about 197.3 kcal mol^{-1} (Table S3). The dissociation of the ΔE_{int} values

into the Pauli repulsion ΔE_{Pauli} and the three attractive components shows that roughly 64.5% comes from the electrostatic attraction (ΔE_{elstat}) while ~32.4% from the orbital term ΔE_{orb} and 3.1% from ΔE_{disp} in complex (**I**). In addition, the values of ΔE_{elstat} show that the nature of L→Zn bonds in the complex is more electrostatic. The covalent bonding between two interacting fragments $[ZnPy(R)]^{+}$ and $[L]^{-}$ (Schiff base ligand) in the complex becomes dominant by the calculated deformation densities $\Delta\rho$, which are associated with the important orbital interactions between the corresponding fragments. The EDA-NOCV (energy decomposition analysis- the natural orbital for chemical valence) method makes it possible to calculate the individual contributions of pairwise interactions. Usually, there are only a small number of pairwise interactions that make a significant contribution to ΔE_{orb} (Table S3). Fig. 4 shows the important deformation densities ($\Delta\rho$) and the associated energy values which provide about 74.6% of the overall orbital interactions for [LZnPy(R)] complex. Visual inspection of Fig. 4 indicates that $\Delta\rho 1$, $\Delta\rho 2$, $\Delta\rho 3$, and $\Delta\rho 5$ comes from the Zn←L σ donation from lone pair of N and O atoms of L ligand (Schiff base ligand) to Zn metal ion in complex (**I**). Also in last figure, it seems that the deformation densities $\Delta\rho 3$, represent the Zn←L π-donation (Fig. 4). Note that the colour in Fig. 4 denotes the charge flow, which is from the red to the blue region.

Fig.s 3-4.
Table 4.

5. Molecular docking of DNA, receptor tyrosine kinases (RTKs), nonreceptor tyrosine kinases (ABL and ARG) and EGFR-TKD

Deoxyribonucleic acid (DNA) is a nucleic acid that be one of the main biological targets for the cancer therapy, and many compounds as DNA replication inhibitors exert their anticancer effects through binding to DNA and damage in cancer cells. Also, overexpression or mutational

activation of some members of receptor tyrosine kinases (RTKs) such as epidermal growth factor receptor participate in the development and progression of numerous human malignancies such as gastric cancer, acute myelocytic leukemia and lymphoblastic leukemia (ALL) [58]. Also, the nonreceptor tyrosine kinases (ABL and ARG) express and regulate diverse cellular functions including cell proliferation, growth and survival, invasion, morphogenesis, apoptosis and migration which can lead to cancer. ABL kinase is an important drug target in the treatment and management of various cancers [59]. Computational docking is extremely potential tool design of such metal– based compounds and the development of drugs as new therapeutic targets. Binding affinity between DNA and on co-protein-targeted new drugs is very important in predicting the binding and in-depth knowledge of cancer molecular mechanisms [59, 60]. The lowest-energy values of the binding suggest that they reasonably binds to macromolecules. The docking results are shown as binding free energy in Fig.5a, listed in Table 5, the calculated minimum relative binding energy (ΔG) for complex (**I**) was -7.73 kcal/mol, which determine the stable binding as between DNA receptor and complex. Moreover, Zn (II) complex could bind to the minor groove of DNA by intercalating (Fig 5b.) which would affect the stability of DNA, thus exhibiting the anticancer activities [61-63]. Also, the compound **I** can interact with DNA through H-binding bonds of the NH_2 with the backbone phosphate (2.18 and 2.49 Å). The calculated binding free energies complex (**I**), Afatinib, Erlotinib and Gefitinib with receptor EGFR-TKD are dominated by the vdW_hb_desolv: -6.47, -7.52, -6.58 and -7.18 kcal/mol, respectively (Table 5). The crystal structure of the complex (**I**) with the EGFR-targeted reveals that complex (**I**) binds to EGFR in the activation P-loop (Fig 6a) [64]. Also, drugs of anticancer such as Afatinib, Gefitinib and Erlotinib are docked in the activation P-loop (Fig 6b). In addition to, compound **(I)** exhibite hydrogen interactions with SYS A773 and PRO A770 the key

residues, while Afatinib and Erlotinib interact to MET A769 and SYS A773 the amino acid residues by hydrogen bonds. Results suggest that compound (**I**) can be a therapeutic role in treatment and management of cancer like Afatinib and Gefitinib. The binding free energy ($\Delta G_{binding}$) of the compound **(I)** to ABL/dasatinib complex and the ABL/imatinib complex was obtained as -5.20 and -6.60 kcal/mol, respectively. While the binding free energy of Nilotinib (anticancer drug) for ABL/dasatinib complex and the ABL/imatinib complex is -6.83 and -8.41 kcal/mol and the binding free energy of Imatinib (anticancer drug) for ABL/dasatinib complex and the ABL/imatinib complex is -8.42 and -10.03 kcal/mol, respectively. The hydrogen binding of compound (**I**) interact the amino acid residues of ABL/dasatinib complex (TYR A435) and the ABL/imatinib complex (ALA A395). Our computational studies represented that complex (**I**) will use as tyrosine kinase inhibitor in treatment cancer by inhibition of the epidermal growth factor receptor (EGFR).

Fig.s 5a-b and 6a-b.

Table 5

6. Spectroscopic characterization of the nanoparticle complex (I)

6. 1. FT-IR ZnO nanoparticles

The FT-IR spectrum was used to characterize and also confirm the formation of zinc oxide nanoparticles of the complex (**I**) as a precursor (Fig. S4). The absorption band at about 430 cm^{-1} corresponds to the vibrational Zn-O band [65, 66]. Characteristic bands of the complex are not detected, suggesting that they decomposed completely into zinc oxide phase without impurities.

6.2. X-ray diffraction studies

Fig. S5 shows the XRD pattern of the ZnO nanoparticles obtained via combustion method from the complex (**I**). Eight characteristic diffraction peaks at 2θ = 31.72°, 34.39°, 36.22°, 47.50°,

56.55°, 62.84°, 67.91°, and 69.03° corresponding to (100), (002), (101), (102), (110), (103), (112), and (201) crystal planes can be indexed to Hexagonal ZnO phase with lattice parameters of $a = b$ = 3.250 A° and c = 5.206 A° according to the standard JCPDS card No. 36–1451[67]. The crystallite size of ZnO was calculated using the Scherrer's equation ($d_{XRD} = 0.9\,\lambda\,/\beta\,(\cos\theta)$) [68], where D, λ, θ, and β are the average crystalline size, the X-ray wavelength of Cu Kα, the Bragg's diffraction angle, and the full width at half maximum (FWHM) of the diffraction peak, respectively. In this pattern, average particle size at main reflection (2θ = 36.22°) was obtained as 36.73 nm. As presented in Table S4, a larger 2θ is caused by the larger crystal size. Also, high purity hexagonal ZnO nanostructure could be obtained via this synthesis method.

6.3. TEM images

The morphology of the ZnO nanoparticles investigated by TEM is presented in Fig S6. Typical TEM image clearly shows that the particles of zinc oxide have a homogeneous and uniform distribution in the rode shape with 5-20 nm width and 20-50 nm length.

7. Conclusion

In this study, the synthesis and characterization of a new complex of Zn(II) was derived from Schiff base ligand and a metal with molar ratio 1:2. The structure of the synthesized complex was determined through their FT-IR, ^{1}H-NMR and UV-Vis data. Moreover, the crystal structure of complex (**I**) was characterized by X-ray. Based on all these data, distorted tetrahedral molecular geometries are suggested for the metal complex. The bonding situation between two interacting fragments, $[ZnPy(R)]^{+}$ and $[L]^{-}$ ligand (Schiff base ligand) in zinc complex, was characterized by NBO and energy-decomposition analysis (EDA), as well as its natural orbitals for chemical valence variation (EDA-NOCV). The ETS-NOCV schemes demonstrated that the

ΔEorb term mainly arises from Zn←L σ donation, while a smaller contribution comes from Zn←L σ-donation. Then, it can be claimed that ZnO nanoparticles were successfully fabricated via combustion synthesis method from complex (**I**). The morphology and crystalline structure of the synthesized zinc oxide nanoparticles were studied by FESEM, TEM, FT-IR, and XRD. As a result, the multifaceted and homogeneous ZnO nanoparticles with appropriate size distribution and hexagonal crystal phase structures were obtained by this approach. Besides, molecular docking techniques were exhibited remarkably that the Zn(II) complex bind to the minor groove of the DNA helix. Also, complex (**I**) will use as tyrosine kinase inhibitor in treatment cancer by inhibition of the epidermal growth factor receptor (EGFR).

Acknowledgements

We thank Semnan University for supporting this study.

References:

[1] M. Salehi, F. Ghasemi, M. Kubicki, A. Asadi, M. Behzad, M. H. Ghasemi, A. Gholizadeh, Inorg. Chimica Acta., 453 (2016) 238-246.

[2] M. Masoudi, M. Behzad, A. Arab, A. Tarahhomi, H. A. Rudbari, G. Bruno, Crystal structures, DFT calculations and Hirshfeld surface analyses of three new cobalt(III) Schiff base complexes derived from meso-1,2-diphenyl-1,2- ethylenediamine, J. Mol. Struct., 1122 (2016) 123-133

[3] A.D. Khalaji, S. Maghsoudlo Rad, G. Grivani, M. Rezaei, K. Gotoh, H. Ishida, Cobalt(III) Complex [CoL3] Derived from an Asymmetric Bidentate Schiff Base Ligand L (L=(5-Bromo-2-hydroxybenzyl-2-furylmethyl)-imine): Synthesis, Characterization and Crystal Structure, Chin. J. Chem., 29 (2011) 1613-1616.

[4] A.A. Osowole, G.A. Kolawole, R. Kempe, O.E. Fagade, Synth. React. Ni(II) and Zn(II) complexes of 2-((thiophen-2-ylmethylene)amino)benzamide: Synthesis, spectroscopic characterization, thermal, DFT and anticancer activities, Inorg. Met.-Org. Nano-Met. Chem. 39 (2009) 165–174.

[5] M.T.H. Tarafder, K.A. Kasbollah Crouse, A.M. Ali, B.M. Yamin, H.-K. Fun, Synthesis and characterization of Zn(II) and Cd(II) complexes of S-benzyl-*β*-N-(2-pyridyl)methylenedithiocarbazate (HNNS): bioactivity of the HNNS Schiff base and its Zn(II), Cu(II) and Cd(II) complexes and the X-ray structure of the $[Zn(NNS)_2]$ complex, Polyhedron. 20 (2001) 2363-2370.

[6] H. A.R. Pramanik, D. Das, P. C. Paul, P. Mondal, Ch. R. Bhattacharjee, Newer mixed ligand Schiff base complexes from aquo-N-(2′-hydroxy acetophenone) glycinatocopper(II) as synthon: DFT, antimicrobial activity and molecular docking study, J. Mol. Struct., 1059 (2014) 309-319

[7] U. M. Rafi, D. Mahendiran, A. Kz. Haleel, R. P. Nankar, M. Doble, A. Kalilur Rahiman, New pyridazine-based binuclear nickel(II), copper(II) and zinc(II) complexes as prospective anticancer agents, New J. Chem,. 40 (2016) 2451-2465.

[8] Sh. Yamada, K. Yamanouch, Metal Complexes of Schiff Bases Obtained from Substituted Salicylaldehydes and 2-Aminopyridine Derivatives, Bull. Chem. Soc. Jpn., 42 (1969) 2562-2566.

[9] C. U. Dueke-Eze, T. M. Fasina, N, Idika, Synthesis, electronic spectra and inhibitory study of some Salicylaldehyde Schiff bases of 2-aminopyridine, Afr. J. Pure Appl. Chem., 5(2) (2011) 13-18.

[10] M. I. Ayad, Sh. A. Sallam, H. E. Mabrouk, Characterization and thermal behaviour of Cu(II) chelates of Schiff bases derived from aminopyridines, Thermochim. Acta, 189 (1991) 65-73.

[11] S. A. Abdel-Latif, H. B. Hassib, Y. M. Issa, Studies on some salicylaldehyde Schiff base derivatives and their complexes with Cr(III), Mn(II), Fe(III), Ni(II) and Cu(II), Spectrochim Acta A Mol Biomol Spectrosc., 67 (2007) 950-957.

[12] N. Tezer, N. Karakus, Theoretical study on the ground state intramolecular proton transfer (IPT) and solvation effect in two Schiff bases formed by 2-aminopyridine with 2-hydroxy-1-naphthaldehyde and 2-hydroxy salicylaldehyde, J Mol Model., 15 (2009) 223–232.

[13] Syntheses and Crystal Structures of a Pair of Trinuclear Cobalt(II) Complexes with the Cations $[Co_3L_4(APYH)_2]$ and $[Co_3L_4(APY)_2]$ (APY 5 2-aminopyridine, L = N-salicylaldehyde-2-iminopyridine), Synth. React. Inorg. Met. Org. Chem., 35 (2005) 193–196.

[14] E. Kahrović, A. Zahirović, S. K. Pavelić, E. Turkušić, A. Harej, In vitro anticancer activity of binuclear Ru(II) complexes with Schiff bases derived from 5- substituted salicylaldehyde and 2-aminopyridine with notably low IC_{50} values, Journal of Coordination Chemistry, 70 (2017) 1683-1697.

[15] S. Giri, S. Biswas, M. G.B. Drew, A. Ghosh, S. K. Saha, Structure and magnetic properties of a tetranuclear Cu(II) complex containing the 2-(pyridine-2-yliminomethyl)-phenol ligand, Inorg Chim Acta., 368 (2011) 152‑156.

[16] G. Tantaru, M.C. Popescu, V. Bild, A. Poiata, G. Lisa, C. Vasile, Spectroscopic, thermal and antimicrobial properties of the copper(II) complex of Schiff base derived from 2-salicylidene) aminopyridine, Appl. Organometal. Chem., 26 (2012) 356‑361.

[17] P. Tyagi, M. Tyagi, S. Agrawal, S. Chandra, H. Ojha, M. Pathak, Synthesis, characterization of 1,2,4-triazole Schiff base derived 3d-metal complexes: Induces cytotoxicity in HepG2, MCF-7 cell line, BSA binding fluorescence and DFT study, Spectrochim Acta A Mol Biomol Spectrosc., 171 (2017) 246-257.

[18] Z. Kazemi, H. Amiri Rudbari, V. Mirkhani, M. Sahihi, M. Moghadam, Sh. Tangestaninejad, Mohammadpoor-Baltork I., Synthesis, characterization, crystal structure, DNA- and HSA-binding studies of a dinuclear Schiff base Zn(II) complex derived from 2-hydroxynaphtaldehyde and 2-picolylamine, J. Mol. Struct., 1096 (2015) 110-120.

[19] A.A. Tomchenko, G.P. Harmer, B.T. Marquis, J.W. Allen, Semiconducting metal oxide sensor array for the selective detection of combustion gases, Sens. Actuators B., 93 (2003) 126-134.

[20] G. Marcì, V. Augugliaro, M.J. López-Muñoz, C. Martín, L. Palmisano, V. Rives, M. Schiavello, R.J.D. Tilley, Time-dependent density functional calculations of ligand K-edge X-ray absorption spectra, Inorg. chim acta,. 105 (2001) 1033-1040.

[21] A. Ghosh, S.K. Das, J.R. Biswas, H.S. Tripathi, G. Banerjee, The effect of ZnO addition on the densification and properties of magnesium aluminate spinel, Ceram. Int., 26 (2000) 605-608.

[22] P. Tonto, O. Mekasuwandumrong, S. Phatanasri, V. Pavarajarn, P. Praserthdam, Preparation of ZnO nanorod by solvothermal reaction of zinc acetate in various alcohols, Ceram. Int., 34 (2008) 57–62.

[23] J. Wang, N. Shi, Y. Qi, M. Liu, Reverse micelles template assisted fabrication of ZnO hollow nanospheres and hexagonal microtubes by a novel fast microemulsion-based hydrothermal method, J. Sol-Gel Sci. Technol., 53 (2009) 101–106.

[24] L. Shen, N. Bao, K. Yanagisawa, A. Gupta, K. Domen, C. A. Grimes, Controlled Synthesis and Assembly of Nanostructured ZnO Architectures by a Solvothermal Soft Chemistry Process, Crystal Growth & Design, 7 (12) (2007) 2742-2748.

[25] H.Y. Yue, W.D. Fei, Z.J. Li, L.D. Wang, Sol–gel process of ZnO and $ZnAl_2O_4$ coated aluminum borate whiskers, J. Sol-Gel Sci. Technol., 44 (2007) 259–262.

[26] P. Jajarmi, Fabrication of pure ZnO nanoparticles by polymerization method, Mater. Lett., 63 (2009) 2646–2648.

[27] A. Moballegh, H.R. Shahverdi, R. Aghababazadeh, A.R. Mirhabibi, ZnO nanoparticles obtained by mechanochemical technique and the optical properties, Surf. Sci., 601 (2007) 2850–2854.

[28] J. M. Grill, J. H. Reibenspies, S. A. Miller, Racemic and chiral expanded salen-type complexes derived from biphenol and binaphthol: Salbip and salbin, J. Organomet. Chem., 690 (2005) 3009.

[29] CrysAlisPro 1.171.38.34a (Rigaku OD, 2015).

[30] A. Altomare, G. Cascarano, C. Giacovazzo and A. Gualardi, J. Appl. Crystallogr. 26 (1993) 343.

[31] G. M. Sheldrick, Acta Crystallogr. C71 (2014) 3-8.

[32] A.D. Becke, Phys. Rev. A 38 (1988) 3098-3100.

[33] J.P. Perdew, Phys. Rev. B. 33 (1986) 8822-8824.

[34] A. Schäfer, H. Horn, R. Ahlrichs, J. Chem. Phys. 97 (1992) 2571-2578.

[35] M.J. Frisch, et al., Gaussian 03, Revision C.01. Gaussian, Inc., Wallingford CT, 2003.

[36] S. J. Sabounchei, M. Pourshahbaz, S. Salehzadeh, M. Bayat, R. Karamia, M. Asadbegy, H. R. Khavasi, New chlorine bridged binuclear silver(I) complexes of bidentate phosphorus ylides: Synthesis, spectroscopy, theoretical and anti-bacterial studies, Polyhedron. 85 (2015) 652–664.

[37] S. J. Sabounchei, H. Nemattalab, S. Salehzadeh, S Khani, M. Bayat, H.R. Khavasi, New chlorine bridged binuclear silver(I) complexes of bidentate phosphorus ylides: Synthesis, spectroscopy, theoretical and anti-bacterial studies, Polyhedron. 27 (2008) 2015-2021.

[38] H. Keypour, N. Rahpeyma, M. Rezaeivala, P. Arzhangi, M. Bayat, L. Valencia, Y. Elerman, O. Büyükgüngör, Synthesis and structural characterization of a new Schiff base macrocyclic

ligand containing a piperazine head unit and its metal complexes. Crystal structure of the Co(II) complex, Polyhedron. 51 (2013) 117–122.

[39] H. Keypour, A. Shooshtari, M. Rezaeivala, M. Bayat, H. Amiri Rudbari, Synthesis and characterization of new Mn(II) and Cd(II) Schiff base complexes containing homopiperazine moiety: Spectral, X-ray crystal structural and theoretical studies, Inorg. Chim. Acta., 440 (2016) 139–147.

[40] H. Keypour, M. Rezaeivala, A. Ramezani-Aktij, M. Bayat, N. Dilek, H. Ünver, New macrocyclic schiff base complexes incorporating a homopiperazine unit: Synthesis of some Co(II), Ni(II),Cu(II) and Zn(II) complexes and crystal structure and theoretical studies, Mol. Struc., 1115 (2016) 180e186.

[41] R. E. Malekshah, M. Salehi, M. Kubickib, A. Khaleghian, Synthesis, structure, computational modeling and biological activity of two new Casiopeınas® Complexes and their nanoparticles, J. Coord. Chem., 72 (2019) 1697–1714.

[42] P. Roozbahani, M. Salehi, R. E. Malekshah, M. Kubicki, Synthesis, crystal structure, electrochemical behavior and docking molecular of poly-nuclear metal complexes of Schiff base ligand derived from 2-amino benzyl alcohol, Inorganica Chimica Acta,. (2019) 119022.

[43] B. Dojer, A. Pevec, P. S˘ egedin, Z. Jaglic˘ic, C. Stropnik, M. Kristl, M. Drofenik, Cobalt(II) coordination compounds with acetate and 2-aminopyridine ligands: Synthesis, characterization, structures and magnetic properties of two polymorphic forms, Inorg. Chim. Acta., 363 (2010) 1343–1347.

[44] C. Yenikaya, M. Poyraz, M. Sarı, F. Demirci, H. Ilkimen, O. Büyükgüngör, Synthesis, characterization and biological evaluation of a novel Cu(II) complex with the mixed ligands 2,6-pyridinedicarboxylic acid and 2-aminopyridine, Polyhedron. 28 (2009) 3526–3532.

[45] Z.M. Zaki, S.S. Haggag, A.A. Soayed, Synthesis,spectral characterization and DNA cleavage studies of Co(II), Ni(II), Cu(II), Zn(II), Cd(II) and Hg(II) complexes with benzofuran2-carbohydrazide schiff bases, Spectro. Lett. 31 (4) (1983) 757.

[46] L.J. Bellamy, The Infrared Spectra of Complex Molecules, second ed., J. Wiley, New York, 1964.

[47] I.C. Mendes, J.P. Moreira, A.S. Mangrich, S.P. Balena, B.L. Rodrigues, H. Beraldo, Coordination to copper(II) strongly enhances the in vitroantimicrobial activity of pyridine-derived N(4)-tolyl thiosemicarbazones, Polyhedron. 26 (2007) 3263–3270.

[48] I.C. Mendes, J.P. Moreira, N.L. Speziali, A.S. Mangrich, J.A. Takahashi, H. Beraldo, *N*(4)-tolyl-2-benzoylpyridine thiosemicarbazones and their copper(II) complexes with significant antifungal activity. Crystal structure of *N*(4)-para-tolyl-2-benzoylpyridine thiosemicarbazone, J. Braz. Chem. Soc. 17 (2006) 1571–1577.

[49] S. Rao, Magneto-Spectral and Biological Studies of Manganese (II) Complexes complexes with Heteroaroyl Hydrazones, Asian J. Chem. 17 (2005) 2663.

[50] M. Odabaşoğlu, F. Arslan, H. Ölmez, O. Büyükgüngör, Synthesis, crystal structures and spectral characterization of trans-bisaquabis(o-vanillinato)copper(II), cis-aquabis(o-vanillinato)copper(II) and aqua[bis(o-vanillinato)-1,2-ethylenediimin]copper(II), Dyes Pigments 75 (2007) 507.

[51] H. Nseimi, J. Safari, A. Heidarnezhad, Synthesis of Schiff base ligands derived from condensation of salicylaldehyde derivatives and synthetic diamine, Dyes Pigments 73 (2007) 251.

[52] A. A. El-Sherif, T.M.A. Eldebss, Synthesis, spectral characterization, solution equilibria, in vitro antibacterial and cytotoxic activities of Cu(II), Ni(II), Mn(II), Co(II) and Zn(II) complexes with Schiff base derived from 5-bromosalicylaldehyde and 2-aminomethylthiophene, Eldebss, Spectrochim. Acta Part A., 79 (2011) 1803.

[53] K. Morokuma. Molecular Orbital Studies of Hydrogen Bonds. III. C=O···H–O Hydrogen Bond in $H_2CO\cdots H_2O$ and $H_2CO\cdots 2H_2O$, Chem. Phys. 55 (1971) 1236-1244.

[54] T. Ziegler, A. Rauk, On the calculation of bonding energies by the Hartree Fock Slater method, Theor. Chim. Acta. 46 (1977) 1-10.

[55] G. Frenking, K. Wichmann, N. Fröhlich, C. Loschen, M. Lein, J. Frunzke, V.c.M. Rayón, Towards a rigorously defined quantum chemical analysis of the chemical bond in donor–acceptor complexes, Coord. Chem. Rev. 238–239 (2003) 55-82.

[56] M. Lein, A. Szabo, A. Kovacs, G. Frenking, Energy decomposition analysis of the chemical bond in main group and transition metal compounds, Farad. Dis. 124 (2003) 365-378.

[57] M. Lein, G. Frenking, The nature of the chemical bond in the light of an energy decomposition analysis, Chapter 13, Elsevier, Amsterdam, (2005) 291-372.

[58] M. Shabani, H. Asgarian-Omran, P. Vossough, R. A. Sharifian, M. Faranoush, S. Ghragozlou, J. Khoshnoodi, A. Roohi, M. Jeddi-Tehrani, H. Mellsted, H. Rabbani, Fazel Shokri (2017) Leukemia & Lymphoma 49 (7) 1360–1367.

[59] B. H. Ha, M. A. Simpson, A. J. Koleske, T. Structure of the ABL2/ARG kinase in complex with dasatinib, J. Boggon (2015) Acta Cryst F71, 443–448.

[60] M. Salehi, M. Kubicki, M. Galini, M. Jafari, R. E. Malekshah, Synthesis, characterization and crystal structures of two novel sulfa drug Schiff base ligands derived sulfonamide and molecular docking study, J. Mol. Struct., 1180 (2019) 595-602.

[61] R. E. Malekshah, M. Salehi, M. Kubicki, A. Khaleghian, Crystal structure, molecular docking, and biological activity of the zinc complexes with 2-thenoyltrifluoroacetone and N-donor heterocyclic ligands, J. Mol. Struct., 1150 (2017) 155–165.

[62] E. Gao, N. Sun, Sh. Zhang, Y. Ding, X. Qiu, Y. Zhan, M. Zhu, Synthesis, structures, molecular docking, cytotoxicity and bioimaging studies of two novel Zn(II) complexes, Eur. J. Med. Chem., 121 (2016) 1–11.

[63] Z. Mandegani, Z. Asadi, M. Asadi, H. R. Karbalaei-Heidari, B. Rastegari, Synthesis, characterization, DNA binding, cleavage activity, cytotoxicity and molecular docking of new nano water-soluble $[M(5\text{-}CH_2PPh_3\text{-}3,4\text{-salpyr})](ClO_4)_2$ (M = Ni, Zn) complexes, Dalton Trans., 45 (2016) 6592-6611.

[64] C.H. Yun, T. J. Boggon, Y. Li, Michele S. Woo, H. Greulich, M. Meyerson, M. J. Eck Structures of Lung Cancer-Derived EGFR Mutants and Inhibitor Complexes: Mechanism of Activation and Insights into Differential Inhibitor Sensitivity
Cancer Cell. 11(3) (2007) 217–227.

[65] R.F. Silva, M.E.D. Zaniquelli, Morphology of nanometric size particulate aluminium-doped zinc oxide films, Colliod. Surf., A 198–200 (2002) 551-558.

[66] H. Li, J. Wang, H. Liu, C. Yang, H. Xu, X. Li, H. Cui, Sol–gel preparation of transparent zinc oxide films with highly preferential crystal orientation, Vacuum. 77 (2004) 57-62.

[67] J. Ye, R. Zhou, C. Zheng, Q. Sun, Y. Lv, C. Li, X. Hou, Size-controllable synthesis of spherical ZnO nanoparticles: Size- and concentration-dependent resonant light scattering, Microchem., J. 100 (2012) 61-65.

[68] Azarof L.V, Buerger M.J (1958) The Powder Method in X-ray Crystallography. New York: McGraw-Hill

Table 1. Crystal data, data collection and structure refinement for complex (**I**).

Parameter	Value
Formula weight	436.61
Color and habit	Colorless, prism
Crystal system	Monoclinic
Crystal size, mm	0.10 × 0.15 × 0.25
Space group	$P2_1/c$
a, Å	7.9510(3)
b, Å	21.2732(9)
c, Å	10.2429(4)
α, deg	90
B, deg	101.557(4)
γ, deg	90
V, Å^3	1697.39(12)
Z	4
ρ_{calcd}, g cm^{-3}	1.709
F(000)	872
μ, mm^{-1})	3.812
Number of unique data	3287
Number of restraints	0
Number of parameters	225
Goodness of fit on F2	1.054
R_1, wR_2 (I > 2σ(I))	0.0495, 0.0834
R_1, wR_2 (all data)	0.0364, 0.0777

Table 2. Selected bond lengths (Å) and bond angles (º) for the complex (**I**). Symmetry code: [i] 3/2-x,1/2-y,z.

Complex	Bond lengths (Å)			Bond angles (º)		
	Selected bond	X-ray	Optimized	Selected angle	X-ray	Optimized
	Zn1-O10A(Zn–O_1)	1.959(2)	2.08 (2.02)	N7A-Zn1-O10A(O_1-Zn-N_2)	93.48(10)	89.57 (93.49)
	Zn1-N7A(Zn-N_2)	2.003(3)	2.01 (1.96)	N7A-Zn1-Br1(N_2-Zn-Br_1)	115.85(7)	118.30 (115.86)
	Zn1-N1B(Zn-N_3)	2.022(3)	2.06 (2.00)	O10A-Zn1-Br1(O_1-Zn-Br_1)	108.83(8)	117.03 (108.84)
	Zn1-Br1	2.3824(5)	2.39 (2.38)	O10A-Zn1-N1B(O_1-Zn-N_3)	102.58(10)	98.09 (102.54)
				N7A-Zn1-N1B(N_2-Zn-N_3)	123.16(11)	118.31 (123.14)
				N1B-Zn1-Br1(N_3-Zn-Br_1)	109.61(8)	111.80 (109.62)

Table 3. Hydrogen bond data (Å, º) for complex (**I**).

D	H	A	D-H	H···A	D···A	D-H···A
N2B	H2B1	N1A	0.92 (6)	2.23(6)	3.015(5)	142(4)
N2B	H2B2	$Br1^i$	0.86(5)	2.87(5)	3.649(4)	151(4)
C3B	H3B	$O10A^i$	0.95	2.43	3.356(5)	164
C6B	H6B	O10A	0.95	2.52	3.137(4)	123

Table 4. Wiberg bond indices (WBI) of complex (**I**) at BP86/def2-SVP level of theory.

	WBI
Zn-N_2 (Zn1-N7A)	0.30
Zn-N_3 (Zn1-N1B)	0.30
Zn–O_1 (Zn1-O10A)	0.32
Zn–Br_1	0.60

Table 5. The epidermal growth factor receptor (1M17), the Abelson leukemia virus protein kinase (2GQG) and (2HYY) docking results with the complex Zn (Unit:kcal/mol)

	DNA	**EGFR-TKD**	**2GQG**	**2HYY**
Estimated Free Energy of Binding* (kcal/mol)	-7.73	-6.47	-5.20	-6.60
Final Intermolecular Energy (kcal/mol)	-8.55	-7.36	-6.09	-7.50
vdW + Hbond + desolv Energy (kcal/mol)	-8.44	-7.19	-6.05	-7.51
Electrostatic Energy (kcal/mol)	-0.12	-0.17	-0.04	-0.01
Final Total Internal Energy (kcal/mol)	-1.51	-1.7	-1.68	-1.68
Torsional Free Energy (kcal/mol)	0.82	-0.89	-0.89	-0.89
Unbound System's Energy (kcal/mol)	-1.51	-1.7	-1.68	-1.68

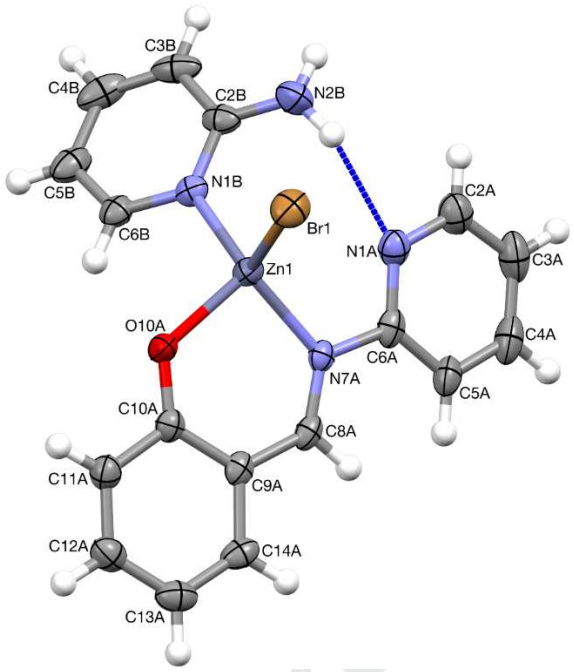

Fig. 1. A perspective view of the complex (**I**); ellipsoids are drawn at the 50% probability level, hydrogen atoms are shown as spheres of arbitrary radii. Intramolecular hydrogen bond is shown as dashed blue line.

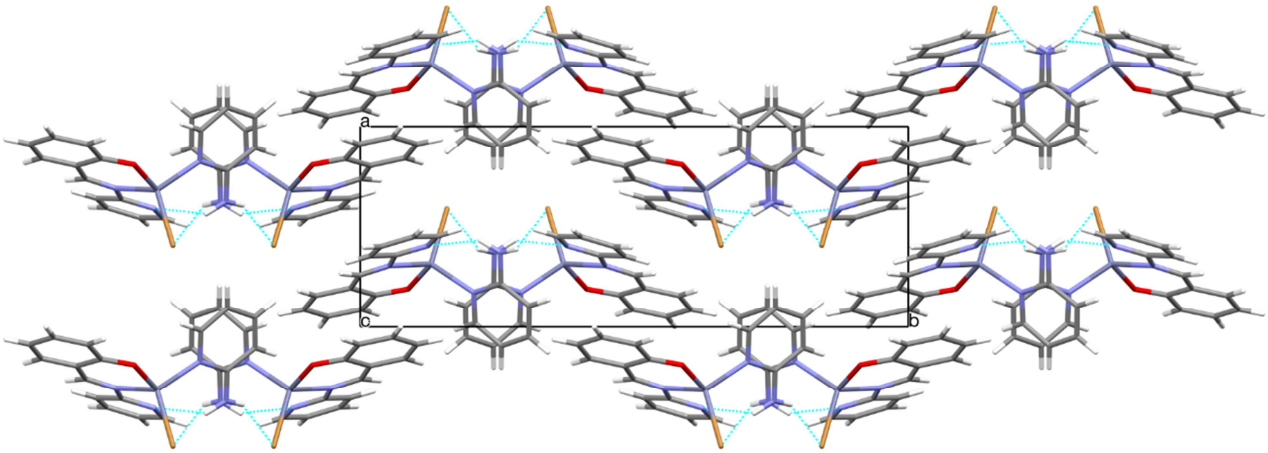

Fig. 2. Crystal structure of complex (**1**), as seen along *z*-direction; hydrogen bonds are shown as thin lines.

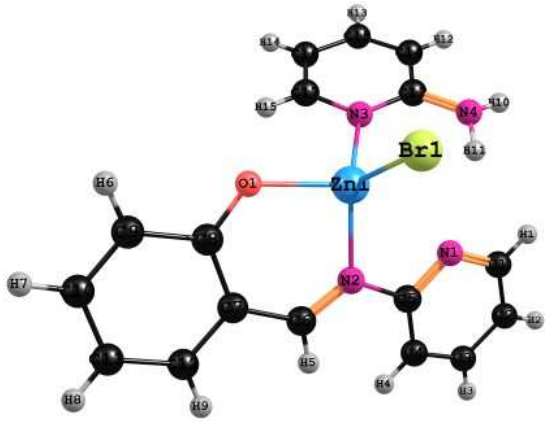

Fig. 3. Optimized geometries of complex (**I**) at BP86/def2-SVP level of theory.

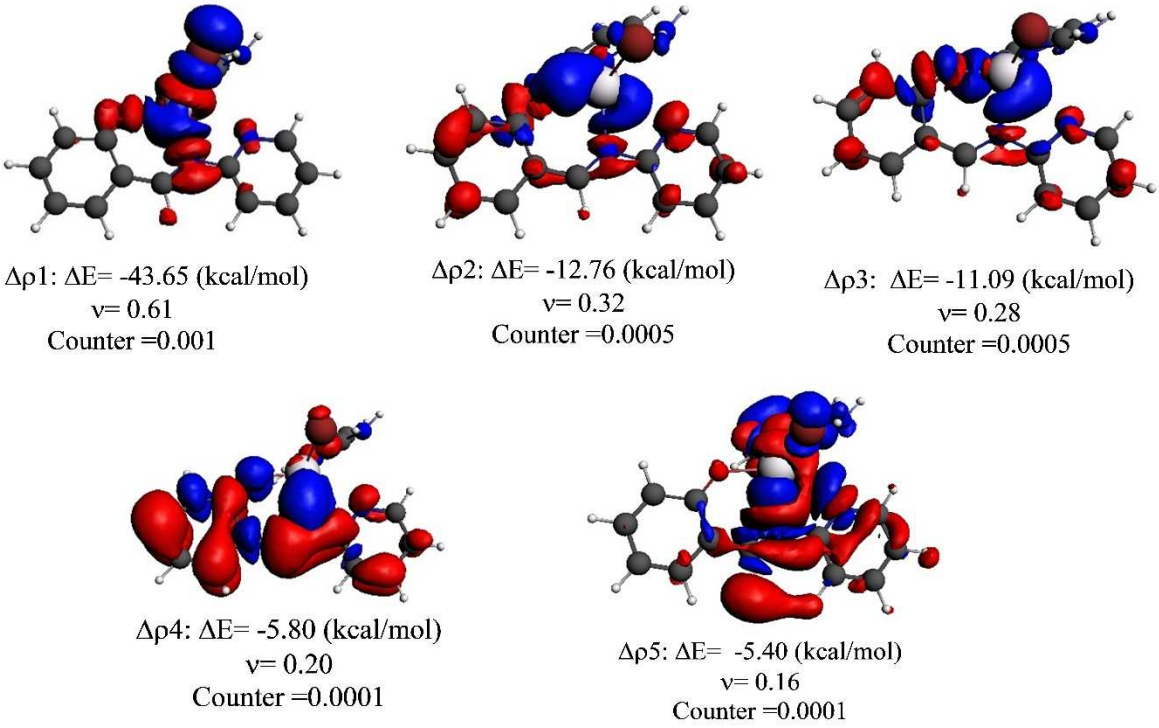

Fig. 4. Deformation densities $\Delta\rho$ associated with the most important orbital interactions in complex (**I**).

.

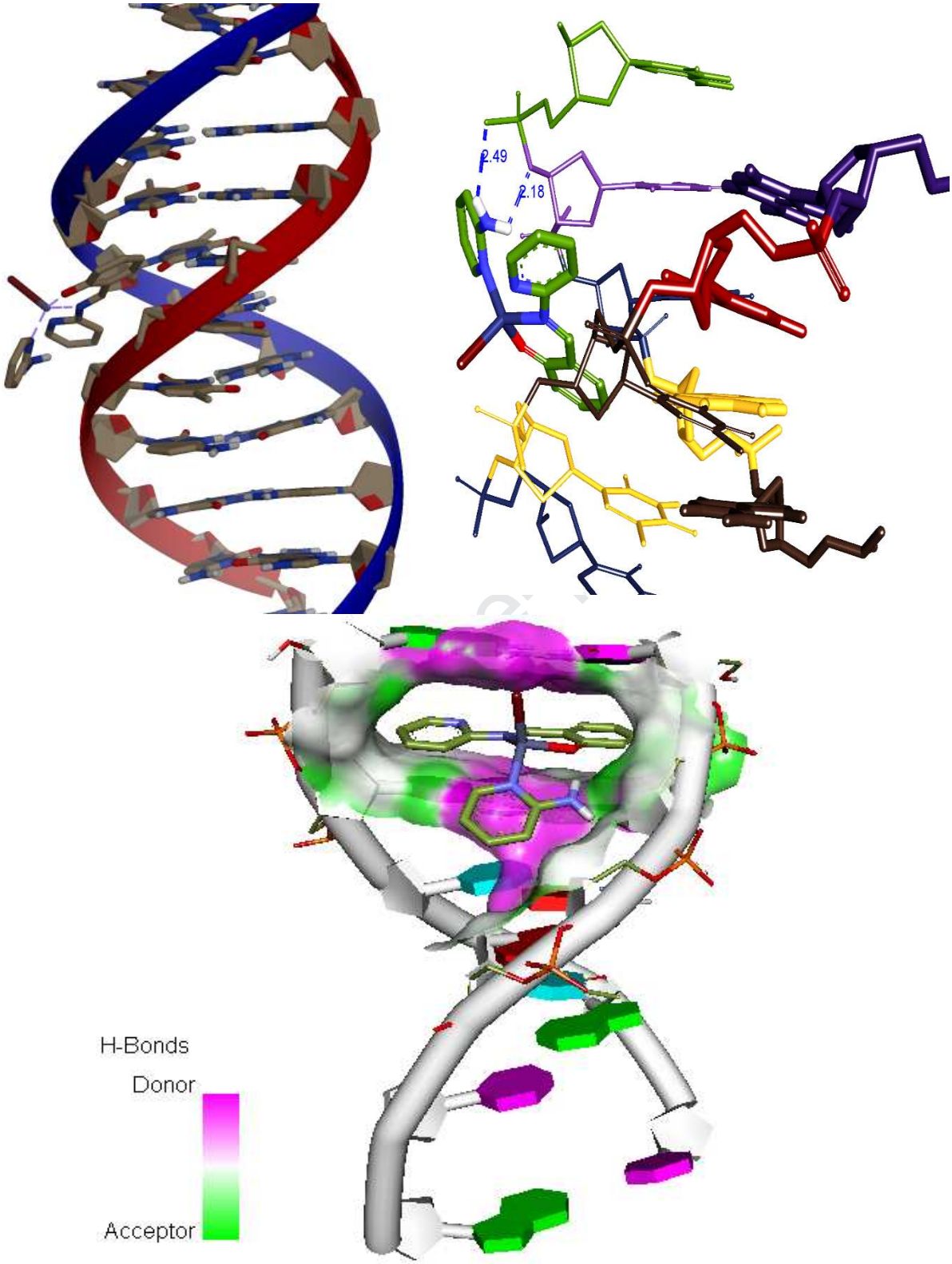

5b

Fig. 5. Docking model and hydrogen bonds of DNA with complex (**I**) **(a),** Docking conformation and intercalation of the compound **(I) (b).**

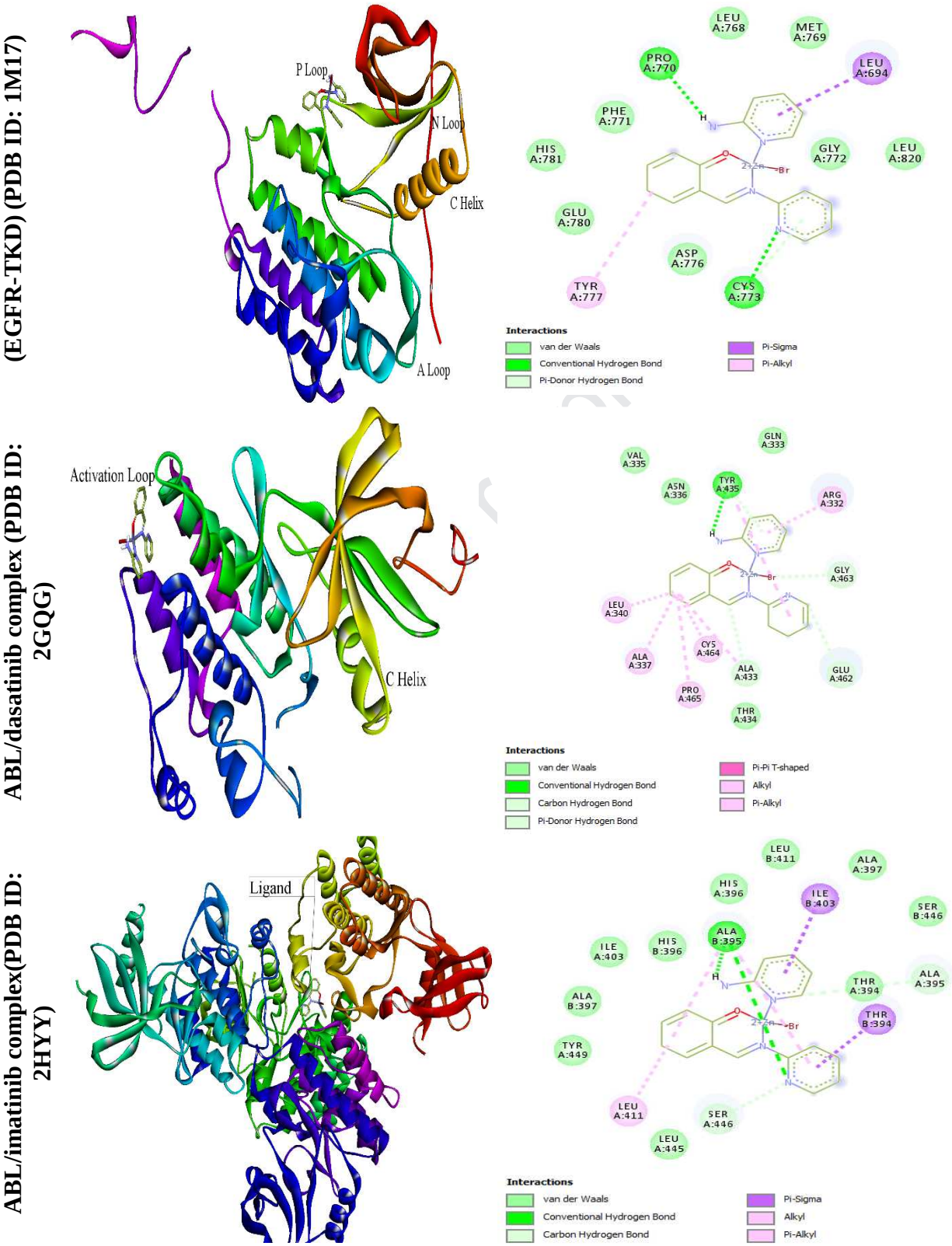

Fig 6a. Docking conformation and bonding interactions of Zn(II) complex with Growth Factor (EGF) Receptor, the ABL/dasatinib complex (PDB ID: 2GQG) and the ABL/imatinib

complex (PDB ID: 2HYY).

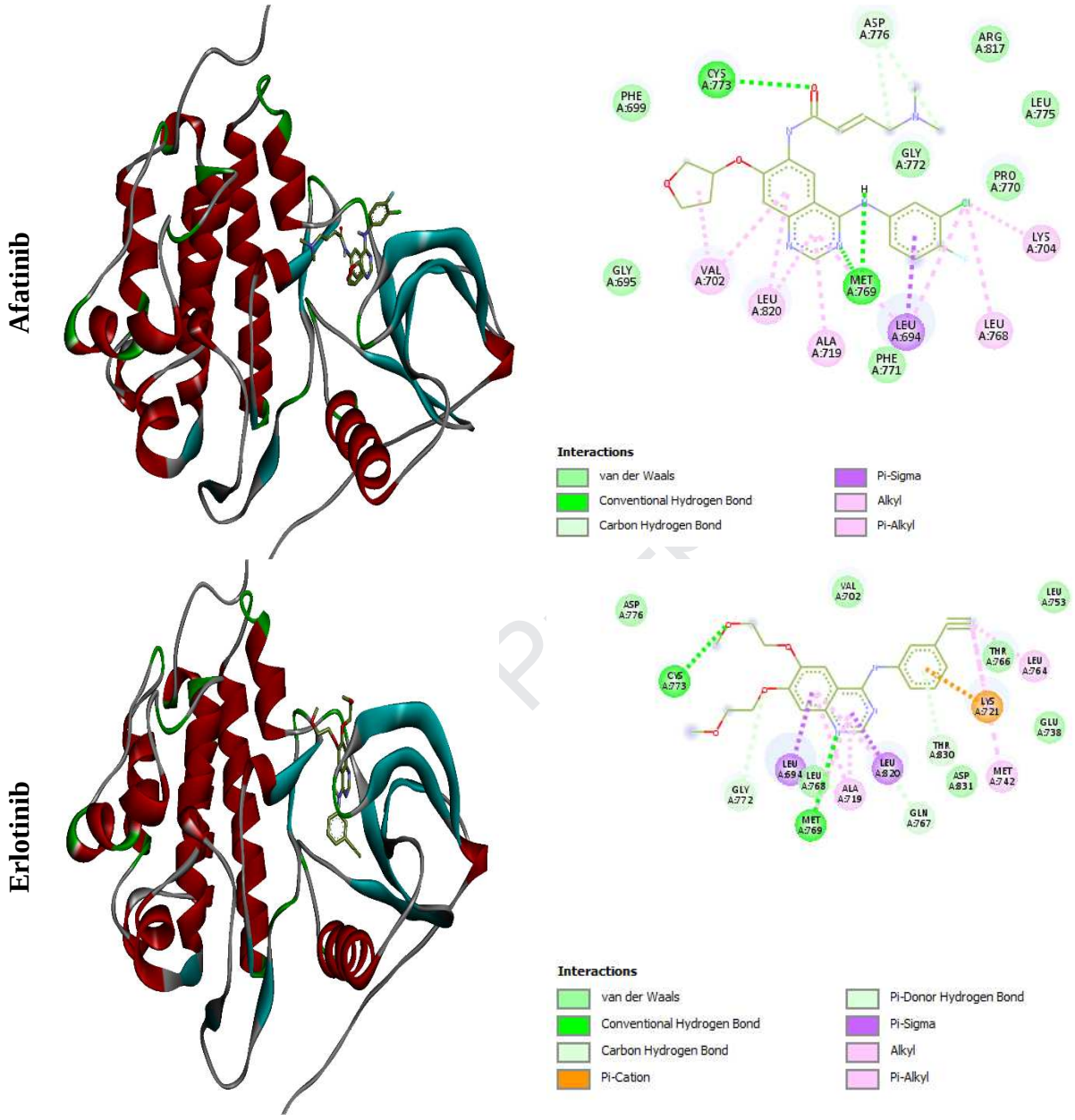

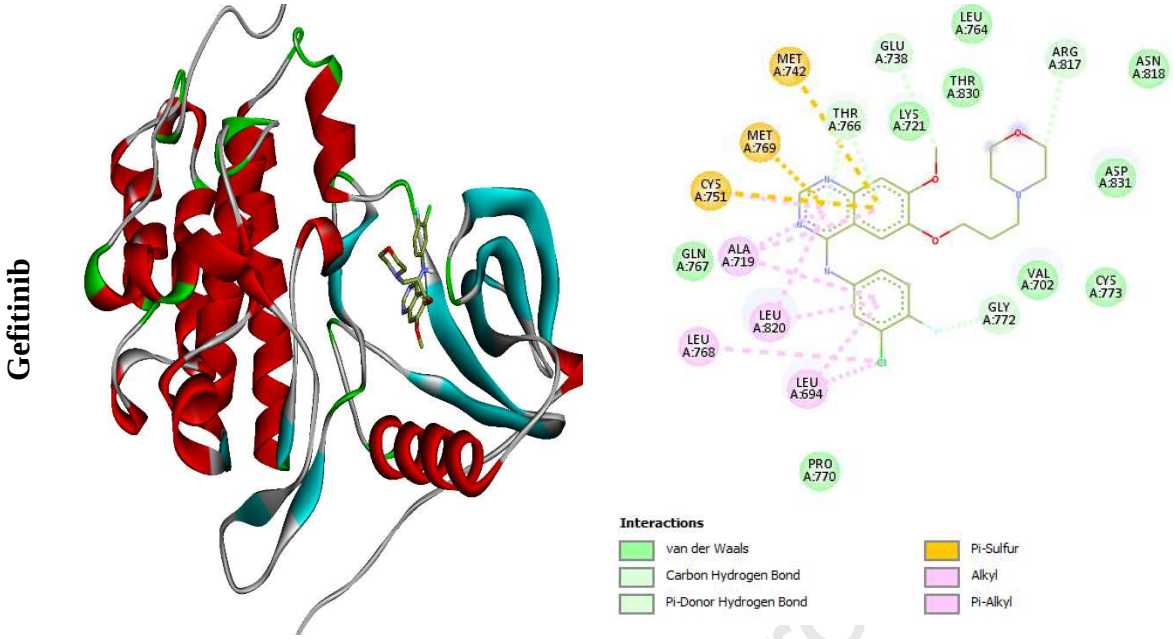

Fig 6b. Docking conformation and bonding interactions of anticancer drugs with Growth Factor (EGF) Receptor.

Highlights

- The crystal structure of Zn(II) was determined by X-ray diffraction.
- Analysis of the bonding in transition metal (TM) complex was studied using NBO and EDA.
- The resulting nanoparticle and their morphology ZnO via combustion method was studied by FT-IR, XRD, FESEM, and TEM.
- The molecular docking of the Zn(II) complex with the epidermal growth factor receptor, the ABL/dasatinib complex and the ABL/imatinib complex was investigated.

Author Contribution Statement

Mehdi Salehi and **Masumeh Galini** carried out the experiment. **Rahime Eshaghi Malekshah** performed molecular simulation study. **Mehdi Bayat** designed the model and the computational framework and analysed the data. Description of the crystal structures performed by **Maciej Kubicki.** All authors discussed the results and contributed to the final manuscript.

Synthesis, structural characterization, DFT and molecular simulation study of new zinc-Schiff base complex and its application as a precursor for preparation of ZnO nanoparticle

Masumeh Galini[a], Mehdi Salehi [a,]*, Maciej Kubicki[b], Mehdi Bayat[c], Rahime Eshaghi Malekshah[a]

[a]*Department of chemistry, Semnan University, Semnan 35351-19111, Iran*

[b]*Faculty of Chemistry, Adam Mickiewicz University, Umultowska 89b, 61-614 Poznan, Poland*

[c]*Department of Inorganic Chemistry, Faculty of Chemistry, Bu-Ali Sina University, Hamedan 65167, Iran*

Declaration of interests

☐ The authors declare that they have no known competing financial interests or personal relationships that could have appeared to influence the work reported in this paper.

☐The authors declare the following financial interests/personal relationships which may be considered as potential competing interests: